ELSEVIER ELSEVIER

Contents lists available at ScienceDirect

Materials Letters

journal homepage: www.elsevier.com/locate/mlblue



A rapid molecular precursor solid-state route to crystalline Fe₂GeS₄ nanoparticles



Po-Yu Hwang ^a, Dominik M. Berg ^{a,b}, Mimi Liu ^a, Cheng-Yu Lai ^a. Daniela R. Radu ^{a,c,*}

- ^a Department of Chemistry, Delaware State University, Dover, DE 19901, USA
- ^b Department of Physics and Astronomy, Rowan University, Glassboro, NJ 08028, USA
- ^c Department of Materials Science and Engineering, University of Delaware, Newark, DE 19716, USA

ARTICLE INFO

Article history: Received 8 January 2018 Received in revised form 6 March 2018 Accepted 4 April 2018 Available online 5 April 2018

Keywords: Nanoparticles Colloidal processing Solar energy materials Electronic materials Fe₂Ge₂S₄

ABSTRACT

Iron germanium sulfide (Fe_2GeS_4) recently emerged as a potential thin film solar photovoltaic absorber. The introduction of the third element—germanium (Ge)—viewed as a solution for overcoming multiple barriers of a photovoltaic pyrite, confers stability to Fe_2GeS_4 at elevated temperatures, typically required for accomplishing grain growth in Gen 2 thin film PV. A facile synthesis of Fe_2GeS_4 nanoparticles from molecular precursors, comprising mechanical mixing of starting materials followed by a two-hour annealing in a sulfur-rich atmosphere is presented herein. Further processing of the resulting Fe_2GeS_4 nanopowders at elevated temperatures demonstrates high thermal stability of Fe_2GeS_4 (up to 500 °C), in comparison with pyrite, which shows onset of pyrrhotite upon heating above 160 °C. Based on the secondary crystalline phases formed, we propose a mechanism of decomposition of Fe_2GeS_4 at high temperatures. Films fabricated with Fe_2GeS_4 were further annealed and revealed that Fe_2GeS_4 withstands high temperatures in thin film.

 $\ensuremath{\text{@}}$ 2018 Elsevier B.V. All rights reserved.

1. Introduction

The search for photovoltaic materials has covered significant grounds from the single crystal silicon, for first generation solar cells, to thin film materials such as CdTe and Cu(In, Ga)Se₂ (CIGS) [1]. While CdTe- and CIGS-based solar cells reached >22.6% power conversion efficiency, the toxicity of some of starting materials along with the high cost and low Earth-abundance of some of the elements, could further impair their competitiveness in solar energy industry [2].

An alternative solution was seen in pursuing sustainable absorber layer PV materials, composed of Earth-abundant elements such as $\text{Cu}_2\text{ZnSn}(S, \text{Se})_4$ (copper zinc tin sulfide–CZTS or sulfo-selenide CZTSSe) or FeS2 (iron sulfide). CZTSSe, benefiting from CIGS similarities, has already proved itself at power conversion efficiencies of 12.6%.

 FeS_2 (pyrite) was suggested to be an excellent PV candidate given its composition and sustainability [3]. Pyrite exhibits an exceptional potential as solar material: high absorption coefficient (> 10^5 cm $^{-1}$, above 1.2–1.4 eV , thus rendering a less than 100 nm thickness need for a thin-film capable of absorbing over 90% of

E-mail address: dradur@desu.edu (D.R. Radu).

the sun's light), good mobility (>300 cm² V⁻¹ s⁻¹ in single crystal form), and a suitable minority carrier diffusion length (100–1000 nm) [4–6]. The attractiveness of 100 nm thin film is visible when compared to 1.5–3.0 μ m for current thin film technologies and > 200 μ m for single-crystal Si cells. Such thin layers not only conserve material, but they also provide an avenue to high efficiency through efficient charge separation associated with a high internal electrical field [7,8].

However, pyrite thin film solar cells, prepared via vacuum processing in the 80's [4,5,9–12] and via solution processing [13–20] in the past five years, did not lead to the predicted expectations. Numerous explanations have emerged, including stoichiometric instability; dependence of conduction type (n or p) on material's surface, crystal size, or film thickness; and pyrite's synthesis conditions [13–20].

Iron chalcogenides Fe₂GeS₄ (FGS) and Fe₂SiS₄ (FSiS), promised a potential alternative to pyrite, by introducing a stabilizing element. A result of theoretical models proposed by Yu et al. Fe₂GeS₄ was reported as a promising photovoltaic material with a band gap suitable for solar absorption (1.4 eV) and high absorption coefficient (10⁻⁵ cm) [7]. The olivine Fe₂GeS₄ crystallographic parameters are showed in Table 1 and its crystal structure in Fig. 1.

Several methods for synthesizing Fe₂GeS₄ nanoparticles have been discussed in recent reports [21–24]. Solution-based syntheses required reacting the precursors in high boiling organic solvents

^{*} Corresponding author at: Department of Chemistry, Delaware State University, Dover, DE 19901, USA.

Table 1Crystallographic parameters of Fe₂GeS₄.

Space group: Pnma, a = 12.467; b = 7.213; c = 5.902, $\alpha = \beta = \gamma = 90^{\circ}$								
Atom	x	у	z	Occupancy				
S	0.4076	0.2500	0.7113	1				
S	0.5729	0.2500	0.2441	1				
S	0.3325	0.0099	0.2520	1				
Ge	0.4110	0.2500	0.0832	1				
Fe	0.0000	0.0000	0.0000	1				
Fe	0.2294	0.2500	0.5067	1				

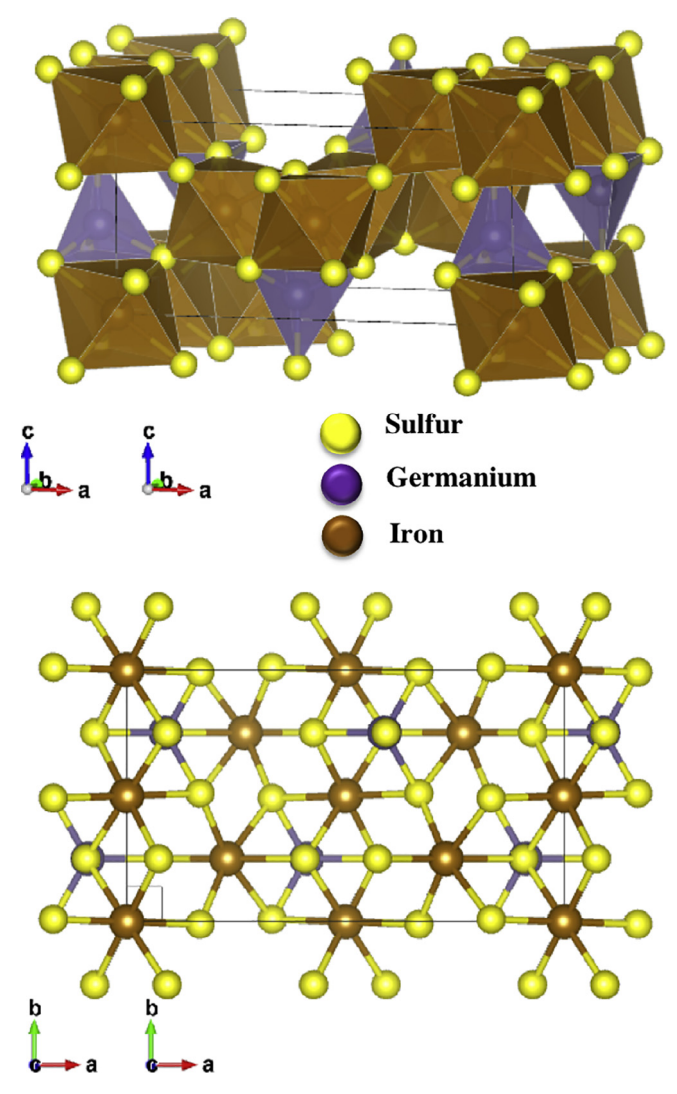


Fig. 1. Crystal structure of Fe₂GeS₄

that act as capping ligands and remain on the nanostructures surface upon reaction; in such approach, the reported reaction times varied from two to twenty-four hours [21,25]. In another report, a solvent free, meccano-chemical approach, involved elemental precursors in a 24 h reactive ball milling process. The reaction occurred as a result of heat generated during the high-energy milling [23].

In the present study, we investigated the ability to obtain high purity Fe_2GeS_4 by a simple and inexpensive solid-state synthesis method which consists of mixing molecular precursors as iron and germanium metal precursors, and elemental sulfur as the sulfur source. We conducted a comprehensive study of the effect of

annealing temperature and the iron precursor on phase purity and crystal growth.

2. Materials and methods

2.1. Chemicals

Iron (II) acetylacetonate (Fe(acac)₂, 99.95%) and ethyl cellulose (EC, 48.0–49.5% (w/w) ethoxy basis) were purchased from Sigma-Aldrich. Iron (II) chloride (FeCl₂, 99.5%), iron (III) chloride (FeCl₃, 98%), and element sulfur (S, 99.5%) were purchased from Alfa Aesar. Ethanol (200 Proof, 100%) and toluene (>99.5%) were purchased from VWR International. The germanium precursor used in the synthesis, Ge[(Gly)₂(H₂O)₂] (Diaquabis(oxoacetato-O,O")ger manium (IV)) (*Ge-Gly*), has been synthesized in house; details of the synthesis are in the Supporting Information (SI).

2.2. Preparation of Fe_2GeS_4 from an Iron Salt, $Ge[(Gly)_2(H_2O)_2]$, and S precursors

Three series of Fe_2GeS_4 preparations: "acac-Gly"; b. "Cl2-Gly", and c. "Cl3-Gly" have been performed. In each preparation, the three precursors in predetermined amounts (Table 2), were mixed by hand-grinding (mortar and pestle) for 10 min, in air. The resulting powders were each immediately annealed in a furnace, in argon atmosphere, for 2 h, in the presence of 1 g of elemental sulfur for each batch, at the following temperatures: $400\,^{\circ}\text{C}$, $450\,^{\circ}\text{C}$, $500\,^{\circ}\text{C}$, $450\,^{\circ}\text{C}$, and $600\,^{\circ}\text{C}$.

2.3. Preparation of Fe₂GeS₄ thin films

The Fe_2GeS_4 nanoparticles obtained in the Cl3-Gly series at $600\,^{\circ}\text{C}$ have been dispersed in various solvents to provide stable dispersions (inks). Details of inks preparation are included in the Supporting Information section. The inks were subsequently coated via a bar-coating method onto quartz substrates; the coated substrates were dried in air and each annealed at $400\,^{\circ}\text{C}$, $450\,^{\circ}\text{C}$, $500\,^{\circ}\text{C}$, and $600\,^{\circ}\text{C}$, respectively.

2.4. Materials characterization

All films and powders were analyzed by Rigaku Miniflex 600 X-ray diffraction system CuKα radiation, set at 30 kV and 10 mA. The measured XRD patterns were further matched to simulated XRD pattern using the Rietveld refinement method on the PDXL software (Rigaku) from which information about the phase composition and crystallite size were determined. More detailed information about the Rietveld Refinement procedure, results, and the ICDD numbers relating to the structural information of each identified phase can be found in the supplementary information document. The Raman spectra were obtained with the XploRa PLUS by Horiba Scientific (532 nm).

Table 2Materials and quantities of reagents used in Fe₂Ge₂S₄ synthesis.

Series	Reagents and	Reagents and amounts used									
	Fe reagent	Fe reagent			Ge reagent			Elemental sulfur			
acac-Gly Cl2-Gly Cl3-Gly	Fe(acac) ₃ FeCl ₂ FeCl ₃	1.4 g 507 mg 648 mg	4 mmol 4 mmol 4 mmol	$\begin{array}{l} \text{Ge}[(\text{Gly})_2(\text{H}_2\text{O})_2\\ \text{Ge}[(\text{Gly})_2(\text{H}_2\text{O})_2\\ \text{Ge}[(\text{Gly})_2(\text{H}_2\text{O})_2 \end{array}$	640 mg 640 mg 640 mg	2.5 mmol 2.5 mmol 2.5 mmol	256 mg 256 mg 256 mg	8 mmol 8 mmol 8 mmol			

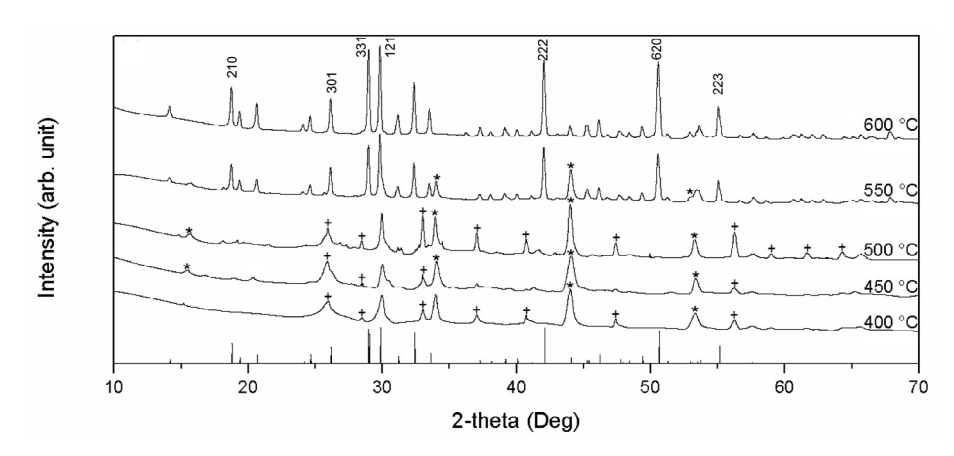


Fig. 2. Compilation of XRD spectra from the Cl₃-Gly series at various annealing temperatures. The impurity symbols are as follows: * for pyrrhotite and + for pyrite. ICDD numbers of each phase are listed in Table 3S in supplementary information.

3. Results and discussion

3.1. Impact of temperature of phase purity for Fe_2GeS_4 obtained from $Fe(acac)_3$, Ge-Gly and S precursors

The XRD patterns indicate a strong dependence of phase purity with annealing temperature. The Rietveld refinement corresponding to each product in the studied series are in Table 1.S (SI) and the XRD data for the series are shown in Fig. 1.S.

Annealing at 400 °C for 2 h leads to the formation of pyrite (FeS₂, marked by the phase percentage of 100%). Starting at 450 °C, Fe₂GeS₄ starts to form (39 ± 3%) together with pyrrhotite (Fe₇S₈, 45 ± 7%) and pyrite (16 ± 6%). FGS becomes the majority phase at 500 °C, while pyrrhotite decreases in relative abundance. At an annealing temperature of 600 °C, FeS₂ completely disappeared, and the formed product is a mixture of the majority phase of Fe₂GeS₄ (72.5 ± 8%) and a minority phase Fe₇S₈ (27.5 ± 1.9%). The estimated crystallite size of Fe₂GeS₄ is 20 nm.

3.2. Impact of temperature on phase purity for Fe_2GeS_4 obtained from $FeCl_2$, Ge-Gly and S precursors

At 400 °C three different phases are present, with greigite (Fe $_3$ S $_4$, 47 ± 5%), pyrrhotite (35 ± 7%), and pyrite (18 ± 3%). Pyrite (69.3 ± 4.8%) replaces greigite as the majority phase at 450 °C and a different phase of pyrrhotite (Fe $_7$ S $_8$, 30 ± 3%) is formed. FGS begins to form around 500 °C as a minority phase (23.8 ± 1.4%) while pyrrhotite (66.0 ± 0.7%) replaces pyrite (10.2 ± 0.7%) as the majority phase. Similar with the trend observed in the acac-Gly series, pyrite disappears completely at 550 °C while FGS percentage (42.4 ± 1.1%) continues to increase. At 600 °C FGS remains the majority phase with 63.9 ± 1.8% while troilite (FeS, 36.1 ± 0.5%) remains as minority phase. The estimated crystallite size of FGS for the Cl $_2$ -Gly series, around 34 nm is slightly larger than that of the acac-Gly series. (see XRD in Fig. 2.S and the Rietveld refinement data in Table 2.S in SI).

$$Fe_{7}S_{2(s)} \longrightarrow Fe_{7}S_{8(s)} \qquad (1)$$

$$Fe_{7}S_{8(s)} + GeS_{2(s)} \longrightarrow Fe_{2}GeS_{4(s)} \qquad (2)$$

$$Fe_{7}S_{8(s)} + Ge_{(s)} \longrightarrow Fe_{2}GeS_{4(s)} \qquad (3)$$

Scheme 1. Proposed mechanism of Fe₂GeS₄ formation.

3.3. Impact of temperature of phase purity for Fe_2GeS_4 obtained from $FeCl_3$, Ge-Gly and S precursors

The annealing study of the third series, using the Cl3-Gly approach, as shown in Fig. 2 and Table 3S (SI), displays a more delayed but also more complete FGS reaction as opposed to the previous two series. At 400 °C and 450 °C, pyrite remains the majority phase with 100% and 73.6%, respectively, while pyrrhotite (8.9 \pm 0.5%) begins to form at 450 °C as a minority phase.

At 500 °C, pyrrhotite (53 \pm 4%) becomes the primary phase as pyrite (47 \pm 3%) decomposes. Even though FGS (71.9 \pm 1.2%) begins to generate and replace pyrrhotite (28.1 \pm 0.9%) only late in the process (at 550 °C), it becomes the single present phase (100 \pm 1. 8%) at an annealing temperature of 600 °C (within the accuracy of the refinement of our measured data). Besides formation of single phase FGS powder, the Cl3-Gly approach results in largest crystallite size of around 36 nm.

3.4. Mechanistic discussion

Despite different evolution of phases within the three studied series, a common trend was observed: the onset of pyrrhotite generation that marks the rapid decomposition of pyrite into pyrrhotite species ($Fe_{1-x}S$) starts at 400 °C which is consistent with the report by Zhang et al. [16]. Iron salts and sulfur can very easily form pyrite at a low temperature which is also the first primary phase we observed at 400 °C [26]. This is consistent with a recent report on solution processed FGS [24].

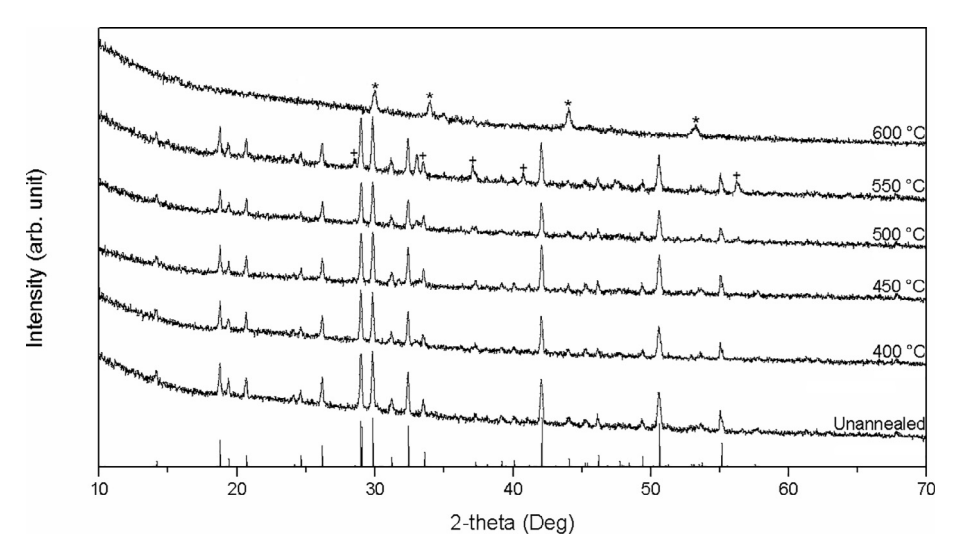


Fig. 3. Compilation of XRD spectra of Fe₂GeS₄ thin films annealed at a variety of temperatures. Symbols: * for pyrrhotite and + for pyrite.

The decomposition of the Ge precursor during annealing could be followed by direct reaction with pyrrhotite, to form FGS (path (3) in the mechanistic Scheme 1). Provided that the reaction occurs in the presence of excess S, GeS₂ could also form, and further react with pyrrhotite, as depicted in Scheme 1. Appearance of peaks indicative of GeS₂ in the XRD spectra were not expected, because germanium sulfide (GeS₂) remains amorphous at low temperatures—as noted by Shimada et al. [27].

Therefore, we hypothesize that the ultimate formation of FGS could follow either path (2) or (3) in the Scheme 1 below (stoichiometric information is not intended here; ratio of reagents is showed in Table 1).

3.5. Temperature stability of Fe₂GeS₄ films

The annealing of films in same conditions as the powder fabrication resulted in well-adherent films. The XRD spectra of films annealed at the showed temperatures in Fig. 3, indicate that the material starts to decompose after reaching 550 °C.

The presence of pyrrhotite—as the first impurity to appear—suggests that the Fe_2GeS_4 decomposition follows the same Scheme 1 mechanism, but in reverse order.

4. Conclusions

The present work proposes a facile and scalable solid-state synthesis approach that generates high stability and high phase purity Fe_2GeS_4 nanoparticles. A detailed study of the impact of annealing temperatures and precursors combination were conducted to determine the optimal conditions that lead to a product with phase purity. Thin films produced with Fe_2GeS_4 nanoparticles obtained by this procedure show high thermal stability, up to $500\,^{\circ}C$, over-performing pyrite stability at high temperatures.

The ability to generate large-grains crystalline Fe₂GeS₄ thin film could, therefore, fulfill the promise of this chalcogenide as a high potential solar absorber.

Acknowledgements

This material is based upon work supported in part by the National Science Foundation under grants No. 1435716, No. 1535876, and No. 1719379 and by the U.S. DOE Sunshot Initiative, Award No. DE-EE0006322. The authors thank Dr. William N. Sha-

farman (Institute of Energy Conversion, UD) for use of their adhesion test setup (Supporting Information).

Appendix A. Supplementary data

Supplementary data associated with this article can be found, in the online version, at https://doi.org/10.1016/j.matlet.2018.04.020.

References

- [1] M.A. Green, The path to 25% silicon solar cell efficiency: history of silicon cell evolution, Prog. Photovoltaics Res. Appl. 17 (2009) 183–189.
- [2] T.K. Todorov, J. Tang, S. Bag, O. Gunawan, T. Gokmen, Y. Zhu, D.B. Mitzi, Beyond 11% efficiency: characteristics of state-of-the-art Cu2ZnSn(S, Se)4 solar cells, Adv. Energy Mater. 3 (2013) 34–38.
- [3] J. Puthussery, S. Seefeld, N. Berry, M. Gibbs, M. Law, J. Am. Chem. Soc. 133 (2011) 716.
- [4] A. Ennaoui, S. Fiechter, C. Pettenkofer, N. Alonso-Vante, K. Bueker, M. Bronold, C. Hoepfner, H. Tributsch, Iron disulfide for solar energy conversion, Sol. Energy Mater. Sol. Cells 29 (1993) 289–370.
- [5] A. Ennaoui, H. Tributsch, Iron sulfide solar cells, Sol. Cells 13 (1984) 197–200.
- [6] G. Smestad, A. Ennaoui, S. Fiechter, W. Hofmann, H. Tributsch, W. Kautek, Thinfilm preparation of semiconducting iron pyrite, Proc. SPIE-Int. Soc. Opt. Eng. 1272 (1990) 67–78.
- [7] L. Yu, S. Lany, R. Kykyneshi, V. Jieratum, R. Ravichandran, B. Pelatt, E. Altschul, H.A.S. Platt, J.F. Wager, D.A. Keszler, A. Zunger, Iron chalcogenide photovoltaic absorbers, Adv. Energy Mater. 1 (2011) 748–753.
- [8] C. Steinhagen, T.B. Harvey, C.J. Stolle, J. Harris, B.A. Korgel, Pyrite nanocrystal solar cells: promising, or fool's gold?, J Phys. Chem. Lett. 3 (2012) 2352–2356.
- [9] A. Ennaoui, S. Fiechter, W. Jaegermann, H. Tributsch, J. Electrochem. Soc. 133 (1986) 97.
- [10] A. Ennaoui, H. Tributsch, Sol. Energy Mater. 14 (1986) 461.
- [11] C. Höpfner, K. Ellmer, A. Ennaoui, C. Pettenkofer, S. Fiechter, H. Tributsch, J. Cryst. Growth 151 (1995) 325.
- [12] G. Smestad, A. Ennaoui, S. Fiechter, H. Tributsch, W.K. Hofmann, M. Birkholz, W. Kautek, Solar Energy Mater. 20 (1990) 149.
- [13] M. Limpinsel, N. Farhi, N. Berry, J. Lindemuth, C.L. Perkins, Q. Lin, M. Law, An inversion layer at the surface of n-type iron pyrite, Energy Environ. Sci. 7 (2014) 1974–1989.
- [14] Y.N. Zhang, J. Hu, M. Law, R.Q. Wu, Effect of surface stoichiometry on the band gap of the pyrite FeS2(100) surface, Phys. Rev. B Condens. Matter Mater. Phys. 85 (2012), 085314/085311-085314/085315.
- [15] A. Baruth, M. Manno, D. Narasimhan, A. Shankar, X. Zhang, M. Johnson, E.S. Aydil, C. Leighton, Reactive sputter deposition of pyrite structure transition metal disulfide thin films: microstructure, transport, and magnetism, J. Appl. Phys. 112 (2012), 054328-054313.
- [16] X. Zhang, T. Scott, T. Socha, D. Nielsen, M. Manno, M. Johnson, Y. Yan, Y. Losovyj, P. Dowben, E.S. Aydil, C. Leighton, Phase stability and stoichiometry in thin film iron pyrite: impact on electronic transport properties, ACS Appl. Mater. Interfaces 7 (2015) 14130–14139.
- [17] J. Hu, Y. Zhang, M. Law, R. Wu, Increasing the band gap of iron pyrite by alloying with oxygen, J. Am. Chem. Soc. 134 (2012) 13216–13219.

- [18] S. Jin, M. Caban-Acevedo, Solar energy conversion and electrocatalysis using earth-abundant pyrite nanomaterials, Prepr. Am. Chem. Soc. Div. Energy Fuels 60 (2015) 589.
- [19] H.A. Macpherson, C.R. Stoldt, Iron pyrite nanocubes: size and shape considerations for photovoltaic application, ACS Nano 6 (2012) 8940–8949.
- [20] J. Puthussery, S. Seefeld, N. Berry, M. Gibbs, M. Law, Colloidal iron pyrite (FeS2) nanocrystal inks for thin-film photovoltaics, J. Am. Chem. Soc. 133 (2010) 716–719.
- [21] S.J. Fredrick, A.L. Prieto, Solution synthesis and reactivity of colloidal Fe2GeS4: a potential candidate for earth abundant, nanostructured photovoltaics, J. Am. Chem. Soc. 135 (2013) 18256–18259.
- [22] D.-H. Lim, P. Ramasamy, J.-S. Lee, Solution synthesis of single-crystalline Fe2GeS4 nanosheets, Mater. Lett. 183 (2016) 65–68.
- [23] B.-I. Park, S. Yu, Y. Hwang, S.-H. Cho, J.-S. Lee, C. Park, D.-K. Lee, S.Y. Lee, Highly crystalline Fe2GeS4 nanocrystals: green synthesis and their structural and optical characterization, J. Mater. Chem. A 3 (2015) 2265–2270.
- [24] M. Liu, D.M. Berg, P.-Y. Hwang, C.-Y. Lai, K.H. Stone, F. Babbe, K.D. Dobson, D.R. Radu, The promise of solution-processed Fe2GeS4 thin films in iron chalcogenide photovoltaics, J. Mater. Sci. 53 (2018) 7725–7734.
- [25] S.A. Orefuwa, C.-Y. Lai, K. Dobson, C. Ni, D. Radu, Novel solution process for fabricating ultra-thin-film absorber layers in Fe2SiS4 and Fe2GeS4 photovoltaics. MRS Online Proceedings Library 2014, 1670.
- [26] F. Jiang, L.T. Peckler, A.J. Muscat, Phase pure pyrite FeS2 nanocubes synthesized using oleylamine as ligand, solvent, and reductant, Cryst. Growth Des. 15 (2015) 3565–3572.
- [27] M. Shimada, F. Dachille, Crystallization of amorphous germanium sulfide and germanium selenide under pressure, Inorg. Chem. 16 (1977) 2094–2097.